Solid Lipid Nanoparticles for Image-Guided Therapy of Atherosclerosis.

Khalid Oumzil, Michael A. Ramin, Cyril Lorenzato, Audrey Hémadou, Jeanny Laroche, Marie Josée Jacobin-Valat, Stéphane Mornet, Claude-Eric Roy, Tina Kauss, Karen Gaudin, et al.

Solid Lipid Nanoparticles for Image-Guided Therapy of Atherosclerosis

Khalid Oumzil[†‡], Michael A. Ramin[†‡], Cyril Lorenzato[§], Audrey Hémadou[§], Jeanny Laroche[§], Marie Josée Jacobin-Valat[§], Stephane Mornet[∥], Claude-Eric Roy[†‡], Tina Kauss[†‡], Karen Gaudin[†‡], Gisèle Clofent-Sanchez[§], and Philippe Barthélémy[*†‡]

† University of Bordeaux, ARNA laboratory, F-33000 Bordeaux, France
‡ INSERM, U869, ARNA laboratory, F-33000 Bordeaux, France
§ CRMSB Centre de Résonance Magnétique des Systèmes Biologiques, UMR 5536, CNRS, University of Bordeaux, F-33076 Bordeaux, France
∥ Institut de Chimie de la Matière Condensée de Bordeaux, ICMCB UPR CNRS 9048, University of Bordeaux, F-33608 Pessac, France

*****E-mail: philippe.barthelemy@inserm.fr

Abstract : Although the application of nanotechnologies to atherosclerosis remains a young field, novel strategies are needed to address this public health issue. In this context, the magnetic resonance imaging (MRI) approach has been gradually investigated in order to enable image-guided treatments. In this contribution, we report a new approach based on nucleoside-lipids allowing the synthesis of solid lipid nanoparticles (SLN) loaded with iron oxide particles and therapeutic agents. The insertion of nucleoside-lipids allows the formation of stable SLNs loaded with prostacycline (PGI2) able to inhibit platelet aggregation. The new SLNs feature better relaxivity properties in comparison to the clinically used contrast agent Feridex, indicating that SLNs are suitable for image-guided therapy.

Introduction

Atherosclerosis is one of the leading causes of death in the developed countries. While the search for efficient treatments continues, it becomes clear that the implementation of new tools combining diagnostic with therapeutic approaches should play an essential role in formulating effective treatment plans.(1-5) Nanoparticles have the ability to carry various therapeutic and/or imaging agents.(6, 7) In this regard, theranostic,(8-10) which combines diagnostic and therapeutic modalities into a single nanosized carrier, has recently emerged as a potential tool for atherosclerosis imaging(11) and treatment.(12) Monitoring disease progression and response to therapy can be followed by magnetic resonance imaging (MRI), which is a noninvasive imaging and diagnostic technique used worldwide in numerous laboratories. This technique is very efficient for imaging soft tissues and provides detailed anatomical images of the body. Ultrasmall superparamagnetic iron oxide (USPIO) particles are maghemite or magnetite nanoparticles currently used as contrast agent in magnetic resonance imaging.(13)
Several promising theranostic systems are currently under investigation and most of these systems involve micelles, liposomes, or polymer-based materials.(14-18) Surprisingly, solid lipid nanoparticles (SLN)(19, 20) loaded with iron oxide nanoparticles have been poorly investigated.
Herein, we report the first example of an SLN featuring both multiple maghemite nanoparticles and an active principle ingredient (API) stabilized by nucleoside-lipids.(21, 22) It is noteworthy that the nucleoside lipids, or nucleolipids, used in these formulations allow the formation of stable SLNs (Figure 1), whereas these nano-objects cannot be obtained using lipids. A nanoprecipitation

procedure was used to generate the SLN loaded with both maghemite nanoparticles and an API such as α-tocopherol or prostacyclin PGI2. The inhibition of platelet activation and aggregation by SLN loaded with prostacyclin was evaluated with the aim of developing a new theranostic tool against atherosclerosis.

Results and Discussion

In a first series of experiments, α-tocopherol was selected as hydrophobic API in order to evaluate the drug loading capability of the SLN. Accordingly, a nucleolipid mixed with α-tocopherol and iron oxide nanoparticles dissolved in ethylic ether was added dropwise to water under stirring. This simple procedure allows the spontaneous formation of the SLNs. In order to investigate the influence of the chemical structure of nucleolipids on the nanocarrier stability, we synthesized SLNs (Figure 1) featuring either positive (SLN^{+} and SLN^{+}_{Toco}) or negative charges (SLN^{-}, SLN^{-}_{peg}, $SLN^{-}_{peg/PGI2}$).

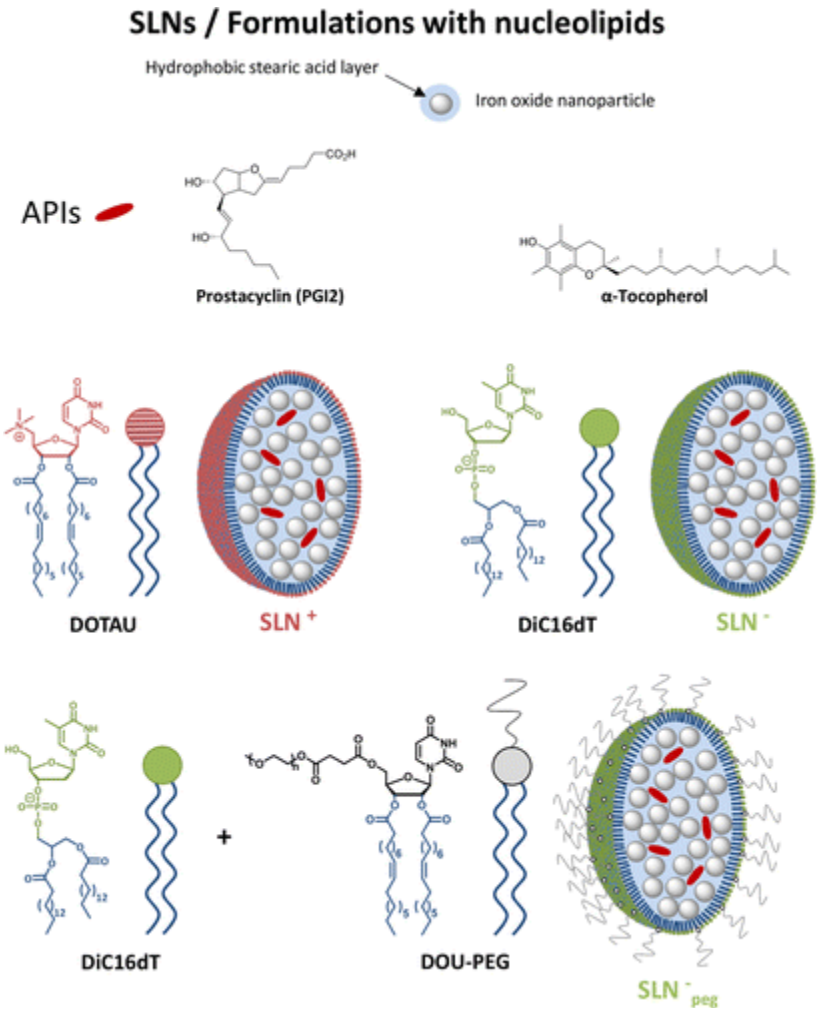

Figure 1. Nucleolipids (DiC16dT: Thymidine 3'-(1,2-dipalmitoyl-sn-glycero-3-phosphate; DOTAU: N-[5'-(2',3'-dioleoyl)uridine]-N',N',N'-trimethylammonium; DOU-PEG: 5'-(O-Methyl-O'-succinylpolyethylene glycol)-2',3'-dioleoyluridine), API, and maghemite used for the implementation of the solid lipid nanoparticles (SLN). SLNs are lipid-based nanocarriers encapsulating grapes of ultrasmall superparamagnetic iron oxide (USPIO) particles and APIs (α-tocopherol or prostacyclin PGI2).

Physicochemical Studies

Dynamic light scattering (DLS) experiments were carried out to confirm the formation of SLNs. Both positive and negative nucleolipids (DOTAU and diC16dT) form similar grapes of nanoparticles in aqueous solution with reasonably narrow polydispersity (PDI = 0.175 and 0.225; diameter = 80 and 98 nm, respectively, Figure 2c). As expected, the zeta potentials of SLN based objects depend on the nucleolipid polar heads (ζ = +55 and −27 mV for SLN^+ and SLN^-). Importantly, a control experiment achieved in the absence of nucleolipid led to the formation of a precipitate, demonstrating that nucleobases are needed to stabilize the SLNs (see Figure SI9). Indeed, it is hypothesized that internucleobase stacking plays an important role in stabilizing the SLN structures. To confirm the base-stacking interactions in the nano-objects, we measured the UV spectra of diC16dT self-assemblies and thymidine in water at room temperature. The molar absorptivity, ε, at 261 nm for the diC16dT self-assemblies is 3.4 mM^{-1} cm^{-1} compared with that for thymidine (ε = 6 mM^{-1} cm^{-1}). This hypochromic effect indicates a different organization of the nucleoside in the nucleolipid self-assemblies compared with thymidine dissolved in water, supporting a stacking arrangement of the pyrimidine bases.

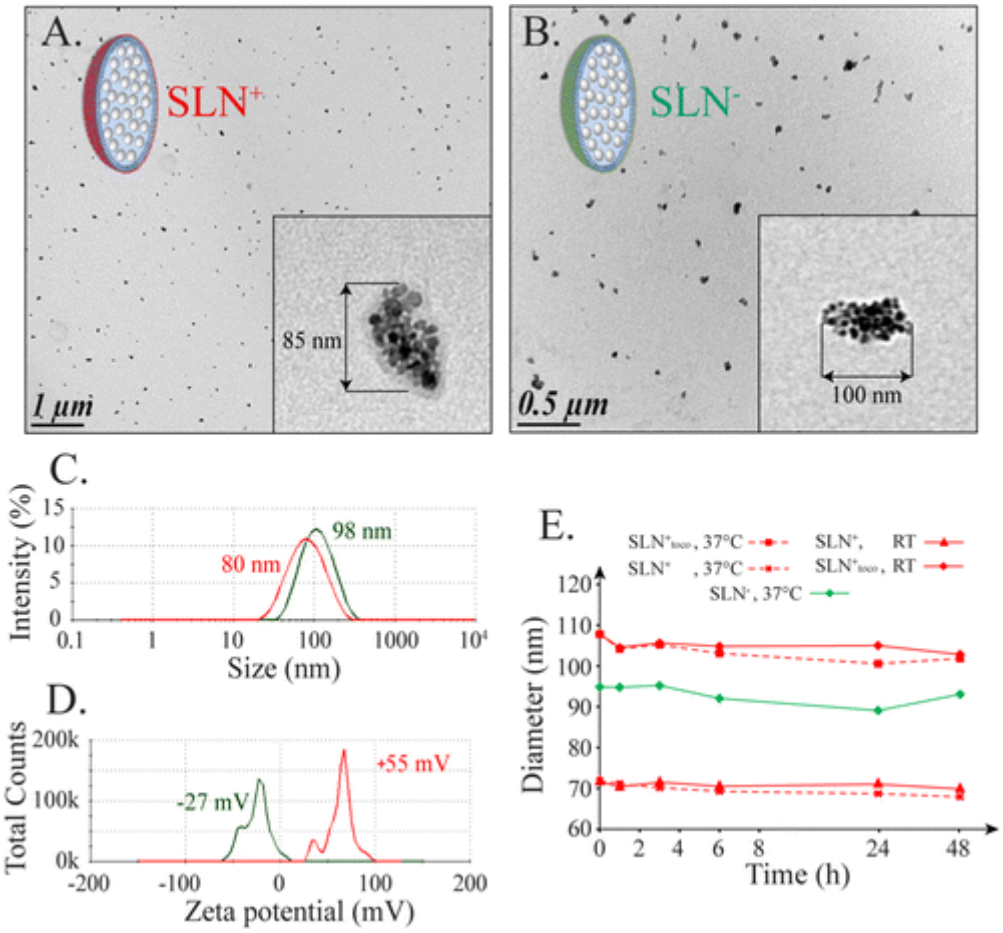

Figure 2. TEM images and schematic representations showing grapes of nanoparticles stabilized either with DOTAU (SLN^+, A) or diC16dT (SLN^-, B). Inset corresponds to a magnification of the TEM images. (C) Size distribution of the SLN^+ (red) and SLN^- (green). (D) Zeta potential of SLN^+ (red) and SLN^-. (E) Colloidal stability versus time at RT and 37 °C.

The presence of polyethylene glycol (Peg) moieties on the surface of nanocarriers has been shown to extend blood-circulation time while diminishing mononuclear phagocyte system uptake (stealth

nanosystems).(23) Hence, SLNs featuring Peg on the surface were synthesized using diC16dT and DOU-PEG. This mixture provides stealth pegylated grapes (SLN^-_{peg}) of 92 nm in diameter and a zeta potential of −23.6 mV (Figures SI7 and SI8). SLNs loaded with different APIs were synthesized. Accordingly, the nanocarriers formulated with cationic nucleolipid DOTAU(24) and α-tocopherol (SLN^+_{Toco}) exhibit a size of 108 nm in diameter and a zeta potential of +49.2 mV (Figures SI10 and SI11). *In fine*, pegylated grapes (loaded with prostacyclin (PGI2) were synthesized using diC16dT and DOU-PEG as nucleolipids ($SLN^-_{Peg/PGI2}$). $SLN^-_{Peg/PGI2}$ show a diameter of 154 nm and a ζ of −22.6 mV (Figures SI13 and SI14).

Transmission electron microscopy (TEM) images of the SLNs were captured (Figure 2A,B). In agreement with the DLS data, both positive and negative nucleolipids self-assemble into similar nano grapes in the presence of iron oxide nanoparticles. Interestingly, similar grapes were observed for different SLNs loaded with APIs (see Figures SI3, SI6, and SI12, for example).

The colloidal stability of SLNs was studied by monitoring the diameter of grapes versus time. The kinetics at room temperature and 37 °C are shown on Figure 2E. The size of all SLNs are not modified for more than 2 days at both room temperature and 37 °C indicating that these nano-objects may be suitable for theranostic applications.

Next we evaluated the drug loading capabilities of the novel formulations. A reverse phase UHPLC method was developed for nucleolipids and α-tocopherol quantification from the SLN composition containing iron oxide nanoparticles. For example, this method allows the separation of the DOTAU and the SLN^+ components within 5 min. Quantification of both DOTAU and α-tocopherol was then possible, which led to the determination of the loading ratios and encapsulation yields. Accordingly, in the case of SLN^+_{Toco} a loading ratio and an encapsulation yield of 42% and 10% were obtained, respectively.

Magnetic Properties of the SLNs

In order to determine whether the nucleolipids based SLNs could be used as MRI contrast agents; we measured the longitudinal (r_1) and the transverse (r_2 and r_2*) relaxivities of the SLNs. Figure 3 shows the transverse relaxation rates (R_2*) of the SLN^- and SLN^+ samples as a function of iron concentration. The theoretical R_2* of the clinically used contrast agents Feridex was plotted for comparison.(25) Both SLN^- and SLN^+ dispersions have higher magnetic properties than those shown by Feridex at the same iron concentrations. Importantly, compared to Feridex (r_2* = 215) the SLN^- and SLN^+ give higher contrast enhancement in MRI as revealed by the relaxivities measured at 4.7 T (r_2* = 557 and 317 s^{-1} mM^{-1}, respectively; see Table SI1).

Inhibition of Platelet Aggregation

Atherosclerosis is a chronic disease of coronary, intracranial, and peripheral arterial diseases, which together account for one of the leading causes of death worldwide. Experimental and clinical studies have shown the possibilities of treating atherosclerosis by bypassing the common method using lipid-lowering drugs. More recent investigations have focused on new classes of nanoparticles capable of detecting(26) and/or counteracting plaque development by acting on the components involved in initiating atherogenesis such as modulators of biologically active lipids, renin-angiotensin-aldosterone system, oxidative stress, and macrophage cholesterol efflux.(27-29) These investigations have been offering new directions in the therapeutic and preventive fields of atherosclerosis. Among biologically active lipids, prostacyclin (PGI2), a major product of COX-2 catalyzed metabolism of arachidonic acid, is a naturally occurring prostaglandin with two potent pharmacological actions: (1) direct vasodilatation of pulmonary and systemic arterial vascular beds, and (2) inhibition of platelet aggregation. Several studies have demonstrated that PGI2 protects against atherothrombosis. Arehart et al. demonstrated that patients harboring a dysfunctional human

prostacyclin receptor variant (R212C) exhibited an enhanced atherothrombotic phenotype.(30) The recent withdrawal of rofecoxib, a selective COX-2 inhibitor, due to increased cardiovascular events further supports the critical role of prostacyclin in inhibiting atherothrombosis in humans.(31, 32) Multiple mechanisms are likely to be involved in the effects of prostaglandins and their receptors on atherosclerosis, including control of platelet activation and aggregation, lipid peroxidation, and leukocyte recruitment into the vessel wall. The huge presence of platelets within the intima of atheroma was recently demonstrated, adding more value to the interest of blocking platelet aggregation for therapeutic purposes.(33) To determine whether SLNs involving both API and an MRI contrast agent would be suitable for atherosclerosis therapy, we examined the effect of SLN loaded with prostacyclin on platelet aggregation. In this work PGI2 was incorporated into diC16dT based SLN^- ($SLN^-_{Peg/PGI2}$; see SI) and activity of PGI2 further tested by aggregometry. Aggregometry experiments measure the ability of various agonists to platelet-rich plasma (PRP) to induce in vitro platelet activation and platelet-to-platelet aggregation. PGI2 analogues can be hydrolyzed at neutral pH in blood and are also subject to enzymatic degradation.(34) Thus, PRP has been incubated with $SLN^-_{Peg/PGI2}$ for 15 min and 3 h to evaluate the maintenance of PGI2 activity. The drug encapsulated in $SLN^-_{Peg/PGI2}$ loaded with iron oxide was able to totally inhibit the aggregation of platelets induced by adenosine 5′-diphosphate (ADP) and thrombin receptor-activating peptide-6 (TRAP-6) at 15 min and 3 h incubation, whereas SLN without API showed a complete aggregation (Figure 4). Effective PGI2 content of SLNs was estimated between 25 and 50 ng/mL (see Figure SI15). These preliminary experiments are of high interest to demonstrate that the activity of PGI2 is preserved in SLN nanoparticles.

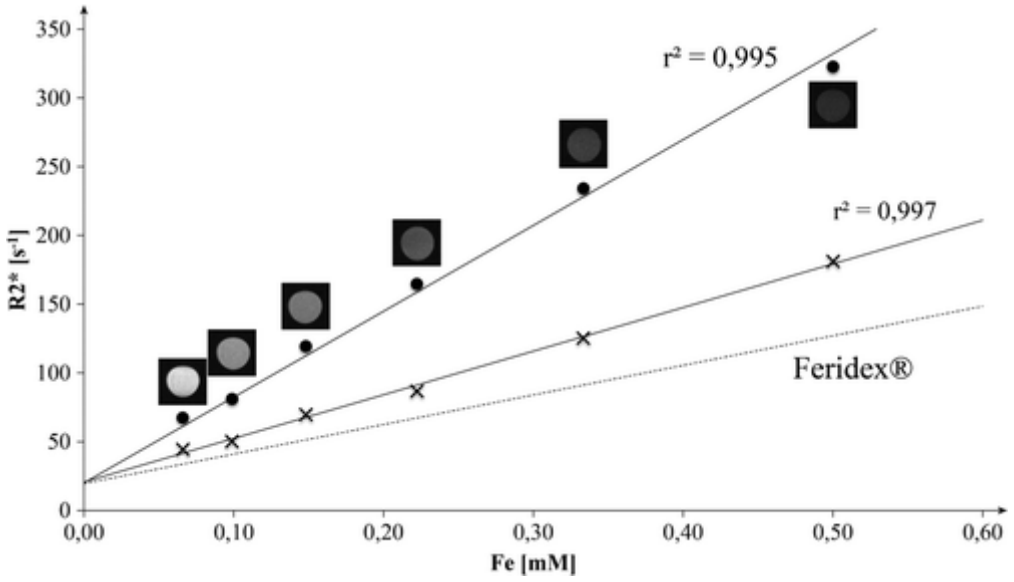

Figure 3. Magnetic resonance relaxometry of SLN^- and SLN^+ at 4.7 T. Transverse relaxation rates (R_2) versus iron concentration for the SLN^- (●) with their corresponding T_1-weighted MRI at TE = 3.5 ms and SLN^+ (×). Linear regression fit was used to extract the relaxivities (solid lines).*

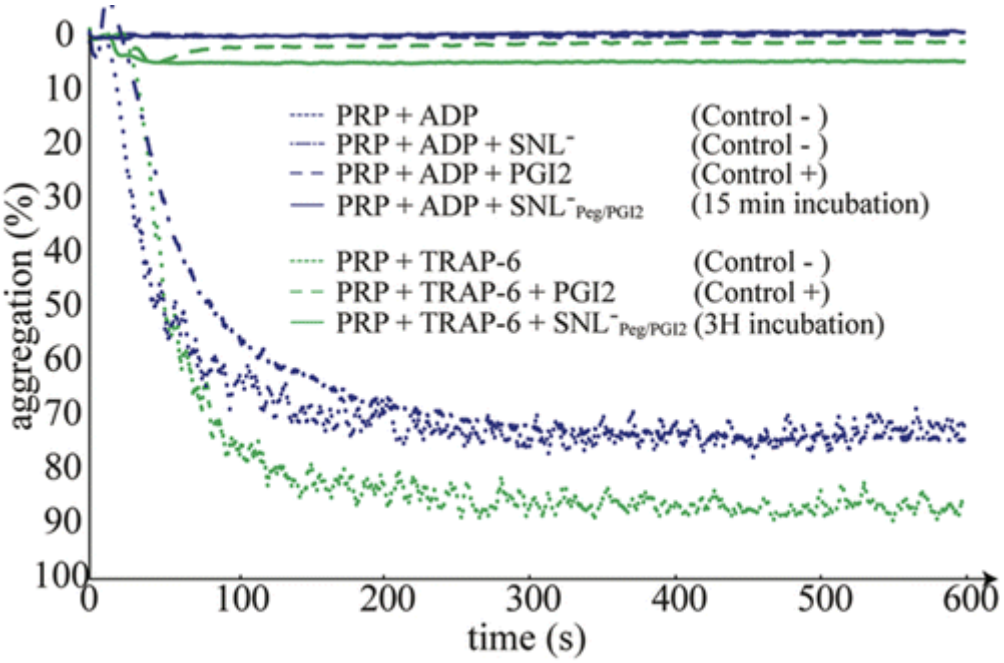

Figure 4. Inhibition of platelet aggregation by $SLN^-_{Peg/PGI2}$. The percentage of aggregation was followed versus time. PRP (207 µL) was stirred in cuvettes at 37 °C and agonists ADP (blue curves) or TRAP-6 (green curves) were added at 5 s to promote platelet aggregation. $SLN^-_{Peg/PGI2}$ (solid lines) as well as free PGI2 totally inhibit the platelet aggregation induced by both ADP (15 min incubation) and TRAP-6 (3 h incubation) agonists, whereas SLN^- nanoparticles, used as negative control (dot-dash line), show complete ADP aggregation.

Conclusion

In this study, we have shown that nucleolipids featuring positive, negative, or neutral polar heads allow for the formation of solid lipid nanoparticles (SLNs) loaded with iron oxide particles and therapeutic agents. Importantly, SLNs cannot be synthesized in the absence of nucleolipids, indicating that the nucleobases are contributing to the stabilization of the grapes. Compared to the clinically used contrast agents Feridex, the SLNs have higher magnetization properties with 2.6-fold higher transverse relaxivity at 4.7 T. It is noteworthy that the insertion of the fragile PGI2 into the SLNs maintains its bioactivity as shown by a complete inhibition of platelet aggregation. Altogether these results indicate that this strategy, added to an antibody-guided addressing scheme, may allow for constructing nanoparticle grapes suitable for theranostic purposes in the field of atherosclerosis.

Experimental Procedures

Preparation of Iron Oxide Nanoparticles Clusters Encapsulated by Nucleolipids

Synthesis of SLN^+ (Encapsulation of Iron Oxide Nanoparticles Clusters by DOTAU)

100 µL of stock solution of positively charged nucleolipid (DOTAU) (50 mg/mL in chloroform) and 20 µL of stock solution of iron oxide nanoparticles coated with stearic acid (10 mg/mL in ether) were mixed. DOTAU was prepared according to Chabaud et al.(24) The organic phase was added dropwise into the aqueous phase (2 mL of Milli-Q Water) placed in a glass tube under stirring by vortex. Then the mixture was placed in a glass flask. Ether was removed under vacuum and the resulting crude material solution was sonicated 3 times (3 × 15 min) and purified on LS columns to

give a pure solution of nanoparticles. The size distribution by intensity measured by dynamic light scattering (DLS) (d = 80 nm) and the zeta potential distribution measured with a 25 MalvernNanoZS device (zeta potential = +55 mV) are shown in Figures SI1 and SI2.

Synthesis of SLN^- (Encapsulation of Iron Oxide Nanoparticles Clusters by diC16dT)

75 µL of stock solution of negatively charged nucleolipid (diC16dT) (50 mg/mL in chloroform), 25 µL of stock solution of 1,2-dioleoyl-*sn*-glycero-3–5 Phosphocholine (DOPC) (Avanti Polar lipids, 50 mg/mL in chloroform) and 20 µL of stock solution of iron oxide nanoparticles (10 mg/mL in chloroform) were mixed. DiC16dT was prepared as reported by Khiaty et al.(36) The organic phase was added dropwise into the aqueous phase (2 mL of Milli-Q Water) placed in a glass tube under stirring by vortex. Then, the mixture was placed in a glass flask. Chloroform was removed under vacuum and the resulting crude material solution was sonicated 3 times (3 × 15 min) and purified on LS columns to give pure solution of nanoparticles. The size distribution by intensity measured by DLS (d = 98 nm) and the zeta potential distribution measured with a MalvernNanoZS device (zeta potential = −27 mV) are shown on Figures SI4 and SI5.

Synthesis of SLN^-_{peg} (Encapsulation of Iron Oxide Nanoparticles Clusters by diC16dT)

75 µL of stock solution of negatively charged nucleolipid (diC16dT) (50 mg/mL in chloroform), 25 µL of stock solution of 1,2-dioleoyl-*sn*-glycero-3–5 phosphocholine (DOPC) (Avanti Polar lipids, 50 mg/mL in chloroform), 30 µL of stock solution of neutral nucleolipid (DOU-PEG2000) (10 mg/mL in chloroform), and 20 µL of stock solution of iron oxide nanoparticles (10 mg/mL in chloroform) were mixed. DiC16dT was prepared as reported by Khiaty et al.(36) DOU-PEG2000 was prepared according to Oumzil et al.(35) The organic phase was added dropwise into the aqueous phase (2 mL of Milli-Q Water) placed in glass tube under stirring by vortex. Then, the mixture was placed in a glass flask. Chloroform was removed under vacuum and the resulting crude material solution was sonicated 3 times (3 × 15 min) and purified on LS columns to give pure solution of nanoparticles. The size distribution by intensity measured by DLS (d = 92 nm) and the zeta potential distribution measured with a MalvernNanoZS device (zeta potential = −23.6 mV) are shown on Figures SI7 and SI8.

Control (DOPC with Iron Oxide Nanoparticles)

100 µL of stock solution of 1,2-dioleoyl-*sn*-glycero-3–5 phosphocholine (DOPC) (Avanti Polar lipids, 50 mg/mL in chloroform) and 20 µL of stock solution of iron oxide nanoparticles (10 mg/mL in chloroform) were mixed. The organic phase was added dropwise into the aqueous phase (2 mL of Milli-Q Water) placed in glass tube under stirring by vortex. Then the mixture was placed in glass flask. Chloroform was removed under vacuum and the resulting crude material solution was sonicated 3 times (3 × 15 min). The iron oxide nanoparticles are not stable in aqueous solution and precipitate (Figure SI9).

Preparation of Iron Oxide Nanoparticles Clusters with Nucleolipid and API

Synthesis of SLN^+_{Toco} (Preparation of a DOTAU Based Nanocarrier Composition Containing Iron Oxide Nanoparticles and α-Tocopherol)

100 µL of stock solution of positively charged nucleolipid (DOTAU) (50 mg/mL in ether), 10 µL of stock solution of α-tocopherol (Sigma-Aldrich, 50 mg/mL in ether), and 20 µL of stock solution of iron oxide nanoparticles (10 mg/mL in ether) were mixed. The organic phase was added dropwise

into the aqueous phase (2 mL of Milli-Q Water) placed in a glass tube under stirring by vortex. Then, the mixture was placed in a glass flask. Ether was removed under vacuum and the resulting crude material solution was sonicated for 3 × 15 min and purified on LS columns to give pure solution of nanoparticles. The size distribution by intensity measured by DLS (d = 108 nm) and the zeta potential distribution measured with a MalvernNanoZS device (zeta potential = +49.2 mV) are shown on Figures SI10 and SI11.

Synthesis of $SLN^{-}_{Peg/PGI2}$ Preparation of a Lipid-Based (diC16dT, DOPC, and DOU-PEG2000) Nanocarrier Composition Containing Iron Oxide Nanoparticles and Prostacyclin (PGI2.Na)

75 µL of stock solution of negatively charged nucleolipid (diC16dT) (50 mg/mL in chloroform + 2% Et_3N), 25 µL of stock solution of DOPC (50 mg/mL in chloroform +2% Et_3N), 30 µL of stock solution of neutral nucleolipid (DOU-PEG2000) (10 mg/mL in chloroform +2% Et_3N), 1 mg of PGI2.Na (Sigma-Aldrich), and 20 µL of stock solution of iron oxide nanoparticles (10 mg/mL in chloroform +2% Et_3N) were mixed. The organic phase was added dropwise into the aqueous phase (2 mL of carbonate–bicarbonate buffer, pH 9.6 at 25 C) placed in glass tube under stirring by vortex. Then the mixture was placed in a glass flask. Chloroform was removed under vacuum and the resulting crude material solution was sonicated for 3 × 15 min and purified on LS column to give a pure solution of nanoparticles. The size distribution by intensity measured by DLS (d = 154 nm) and the zeta potential distribution measured with a MalvernNanoZS device (zeta potential = −22.6 mV) are shown on Figures SI13 and SI14.

Stability Study

Iron oxide nanoparticle clusters encapsulated by DOTAU (SLN^{+}) or diC16dT (SLN^{-}) and DOTAU-based nanocarrier composition comprising iron oxide nanoparticles and α-tocopherol (SLN^{+}_{Toco}) in 500 µL of Milli-Q water were incubated at 37 °C under a 500 rpm stirring. For different times (0, 1, 3, 6, 24, 48 h), particle sizes were determined using a Zetasizer 3000 HAS MALVERN. The results show that the overall sizes, either in the absence or in the presence of therapeutic agents, and either positively or negatively charged, are not modified as a function of time (more than 2 days), which indicates colloidal stability both at room temperature and at 37 °C (see SI).

Preparation of Samples for HPLC Analysis and Dosage of DOTAU and α-Tocopherol (SLN^{+} and SLN^{+}_{Toco})

Pure suspensions of cationic nanoparticles prepared were centrifuged at 14 000 rpm for 15 min in order to remove the supernatant. Cationic nanoparticles (in the form of a pellet) were suspended in ethanol. The resulting solution was mixed for 15 min at RT and centrifuged at 14 000 rpm for 5 min. The supernatant was evaporated and then solubilized in 5 mL of mobile phase follow by a 5× dilution before injection in HPLC (Figure SI18A and B). The precipitate was analyzed by HPLC after solubilization in 5 mL of mobile phase (Figure SI18C and D). A reverse phase UHPLC method was developed for nucleolipid (DOTAU) and α-tocopherol quantification from the lipid-based nanocarrier composition containing iron oxide nanoparticles. This method allows the separation of the DOTAU and API within 5 min for lipid-based (DOTAU) nanocarrier composition. The separation was carried out with a column Syncronis C18 50 × 2.1 mm, 1.7 µm with a mobile phase composed of MeOH + 0.1% HCOOH. The flow rate was set to 0.2 mL/min. The detection was performed at 293 and 260 nm for α-tocopherol and DOTAU, respectively. The injected volume was 1.0 µL, which allowed the detection of DOTAU and α-tocopherol at limit of quantification of 5 ng and 15 ng, respectively. Standard curves for DOTAU and α-tocopherol, as shown on Figures SI15 and SI16, were generated by determining the intensity of signal versus concentrations. The

HPLC analyses are shown in Figure SI18A–D. Figure SI18A and B present supernatant analysis and C and D precipitate analysis. Quantification of both DOTAU and α-tocopherol was then possible, which led to encapsulated recovery and determination of loading ratio values. Loading ratio was 42%; that obtained in the case of a DOTAU/α-tocopherol with a ratio 10:1 for processing and the encapsulated drug recovery was around 10%.

MR Relaxometry

A total number of 8 different concentrations ranging from 0 to 0.5 mM Fe of both SLN^+ and SLN^- were prepared in Eppendorf PCR Tubes (0.5 mL). Transverse images passing through the 8 tubes were acquired on a 4.7 T Bruker Biospin (Billerica, MA) MRI system with a 1H whole body RF volume coil of 35 mm inner diameter and the relaxation rate (R_n) maps were computed using the Paravision 6.0 software. Samples were scanned at 21 °C with a 256 × 192 matrix and a FOV = 40 × 30 mm. R_1 measurements were acquired using the Bruker T_1 map RARE method (TR = 5000, 3000, 1500, 800, 400, 200 ms; TE = 6 ms; RARE factor = 2). Multi-spin–echo (ΔTE = 8.45; number of echoes = 20; TR = 2 s) and gradient-echo (flip angle = 60°; number of echo = 8 ; TE initial = 3.5 ms; ΔTE = 5 ms; TR = 800 ms; flyback) sequences were employed to compute an R_2 map and R_2*map, respectively. The mean relaxation rates, Rn, of each dilution were calculated from ROIs encompassing each tube and plotted versus their corresponding Fe concentrations. A linear regression was used to extract the relaxivity (r_n) of each sample, given as the slope of the resulting line in units of s^{-1} mM^{-1} of Fe.

Analysis of Bioactivity of Encapsulated API

Blood was obtained in a 1/10th volume of 3.8% sodium citrate from healthy volunteers who had not taken any drugs known to affect platelet function for 2 weeks prior to the study. Platelet-rich plasma (PRP) is prepared by centrifugation at 20 °C for 10–15 min at 150–200*g* and stored at room temperature. Platelet-poor plasma (PPP) is prepared by further centrifugation of the remaining plasma at 2700*g* for 15 min and calibrates the 100% light transmission of the aggregometer. PRP (207 μL) was stirred in cuvettes at 37 °C and platelet agonists (ADP (10 μM) or TRAP-6 (100 μM) were added at 5 s to promote platelet aggregation. The in vitro platelet aggregation was determined using a four-channel light transmission aggregometer (APACT 4004, ELITech, France).

Transmission Electronic Microscopy (TEM)

Nanoparticles were visualized by negative staining microscopy. 10 μL aliquots of nanoparticles (1 mM) were transferred to a carbon-coated copper grid for 10 min. The sample was then dried and stained with 2.5% (W/W) of uranyl acetate in water for 5 min. The specimens were observed with a Hitachi H 7650 electron microscope.

Particle Size and Zeta Determination

Particle zeta and size were determined using a Zetasizer 3000 HAS MALVERN. Experiments were realized with 50 μL of the nanoparticles diluted in 1.2 mL of DI water and measurements were performed at 25 °C.

The Supporting Information is available free of charge on the ACS Publications website at DOI: 10.1021/acs.bioconjchem.5b00590.

- DLS data, zeta potentials and TEM of SLNs synthesized in different experimental conditions, HPLC dosages, and MR relaxometry (PDF)

The authors declare no competing financial interest.

Acknowledgment : This work has been supported by two public grants of the French National Agency (ANR) (1) in the frame of the Investments for the Future Program, referenced ANR-10-LABX-57 and named TRAIL (Translational Research and Advanced Imaging Laboratory) MIMATHUMAB and (2) within the context of SVE5 program, named ATHERANOS. The authors thank the Bordeaux Imaging Centre (BIC) for technical assistance during TEM observations.

References.

1. Libby, P., Ridker, P. M., and Hansson, G. K. (**2011**) Progress and challenges in translating the biology of atherosclerosis Nature 473, 317– 325 DOI: 10.1038/nature10146
2. Lobatto, M. E., Calcagno, C., Millon, A., Senders, M. L., Fay, F., Robson, P. M., Ramachandran, S., Binderup, T., Paridaans, M. P., and Sensarn, S. **2015**, Atherosclerotic Plaque Targeting Mechanism of Long-Circulating Nanoparticles Established by Multimodal Imaging ACS Nano 9, 1837– 1847 DOI: 10.1021/nn506750r
3. Melzer, S., Ankri, R., Fixler, D., and Tarnok, A. (**2015**) Nanoparticle uptake by macrophages in vulnerable plaques for atherosclerosis diagnosis J. Biophotonics 8, 871 DOI: 10.1002/jbio.201500114
4. Seo, J. W., Baek, H., Mahakian, L. M., Kusunose, J., Hamzah, J., Ruoslahti, E., and Ferrara, K. W. (**2014**) (64)Cu-labeled LyP-1-dendrimer for PET-CT imaging of atherosclerotic plaque Bioconjugate Chem. 25, 231– 239 DOI: 10.1021/bc400347s
5. Kheirolomoom, A., Kim, C. W., Seo, J. W., Kumar, S., Son, D. J., Gagnon, M. K., Ingham, E. S., Ferrara, K. W., and Jo, H. (**2015**) Multifunctional Nanoparticles Facilitate Molecular Targeting and miRNA Delivery to Inhibit Atherosclerosis in ApoE(−/−) Mice ACS Nano 9, 8885– 8897 DOI: 10.1021/acsnano.5b02611
6. Couvreur, P. (**2013**) Nanoparticles in drug delivery: past, present and future Adv. Drug Delivery Rev. 65, 21– 23 DOI: 10.1016/j.addr.2012.04.010
7. Wolfram, J., Shen, H., and Ferrari, M. (**2015**) Multistage vector (MSV) therapeutics J. Controlled Release 219, 406 DOI: 10.1016/j.jconrel.2015.08.010
8. Luk, B. T., Fang, R. H., and Zhang, L. (**2012**) Lipid- and Polymer-Based Nanostructures for Cancer Theranostics Theranostics 2, 1117– 1126 DOI: 10.7150/thno.4381
9. Ryu, J. H., Lee, S., Son, S., Kim, S. H., Leary, J. F., Choi, K., and Kwon, I. C. (**2014**) Theranostic nanoparticles for future personalized medicine J. Controlled Release 190, 477–484 DOI: 10.1016/j.jconrel.2014.04.027
10. Biswas, S., Kulkami, J. A., Tam, Y. Y., Chem, S., Tam, Y. K., and Cullis, P. (2015) In Next generation magnetic lipid nanohybrids for theranostics, 250th ACS National Meeting, Fall 2015, Boston, MA, Aug 16–20, 2015; American Chemical Society, Washington, DC.
11. von zur Muhlen, C., von Elverfeldt, D., Bassler, N., Neudorfer, I., Steitz, B., Petri-Fink, A., Hofmann, H., Bode, C., and Peter, K. (**2007**) Superparamagnetic iron oxide binding and uptake as imaged by magnetic resonance is mediated by the integrin receptor Mac-1 (CD11b/CD18): Implications on imaging of atherosclerotic plaques Atherosclerosis 193, 102– 111 DOI: 10.1016/j.atherosclerosis.2006.08.048

12. Lobatto, M. E., Fuster, V., Fayad, Z. A., and Mulder, W. J. M. (**2011**) Perspectives and opportunities for nanomedicine in the management of atherosclerosis Nat. Rev. Drug Discovery 10, 835– 852 DOI: 10.1038/nrd3578
13. Zhao, X., Zhao, H., Chen, Z., and Lan, M. (**2014**) Ultrasmall superparamagnetic iron oxide nanoparticles for magnetic resonance imaging contrast agent J. Nanosci. Nanotechnol. 14, 210– 220 DOI: 10.1166/jnn.2014.9192
14. Taylor, R. M., Huber, D. L., Monson, T. C., Ali, M. S., Bisoffi, M., and Sillerud, L. O. (**2011**) Multifunctional iron platinum stealth immunomicelles: targeted detection of human prostate cancer cells using both fluorescence and magnetic resonance imaging J. Nanopart. Res. 13, 4717– 4729 DOI: 10.1007/s11051-011-0439-3
15. Lemon, C. M., Karnas, E., Han, X., Bruns, O. T., Kempa, T. J., Fukumura, D., Bawendi, M. G., Jain, R. K., Duda, D. G., and Nocera, D. G. (**2015**) Micelle-Encapsulated Quantum Dot-Porphyrin Assemblies as in Vivo Two-Photon Oxygen Sensors J. Am. Chem. Soc. 137, 9832– 9842 DOI: 10.1021/jacs.5b04765
16. Al-Jamal, W. T. and Kostarelos, K. (**2011**) Liposomes: from a clinically established drug delivery system to a nanoparticle platform for theranostic nanomedicine Acc. Chem. Res. 44, 1094– 1104 DOI: 10.1021/ar200105p
17. Al-Jamal, W. T., Al-Jamal, K. T., Bomans, P. H., Frederik, P. M., and Kostarelos, K. (**2008**) Functionalized-quantum-dot-liposome hybrids as multimodal nanoparticles for cancer Small 4, 1406– 1415 DOI: 10.1002/smll.200701043
18. Nie, S., Zhang, J., Martinez-Zaguilan, R., Sennoune, S., Hossen, M. N., Lichtenstein, A. H., Cao, J., Meyerrose, G. E., Paone, R., Soontrapa, S., Fan, Z., and Wang, S. (**2015**) Detection of atherosclerotic lesions and intimal macrophages using CD36-targeted nanovesicles J. Controlled Release 220, 61– 70 DOI: 10.1016/j.jconrel.2015.10.004
19. Ekambaram, P., Abdul Hasan Sathali, A., and Priyanka, K. (**2012**) Solid Lipid Nanoparticles: a review Sci. Rev. Chem. Commun. 2, 80– 102
20. Bae, K. H., Lee, J. Y., Park, T. G., and Nam, Y. S. (**2013**) Optically Traceable Solid Lipid Nanoparticles Loaded with siRNA and Paclitaxel for Synergistic Chemotherapy with In situ Imaging Adv. Healthcare Mater. 2, 576– 584 DOI: 10.1002/adhm.201200338
21. Aimé, A., Beztsinna, N., Patwa, A., Pokolenko, A., Bestel, I., and Barthélémy, P. (**2013**) Quantum Dot Lipid Oligonucleotide Bioconjugates: Toward a New Anti-MicroRNA Nanoplatform Bioconjugate Chem. 24, 1345– 1355 DOI: 10.1021/bc400157z
22. Luvino, D., Khiati, S., Oumzil, K., Rocchi, P., Camplo, M., and Barthélémy, P. (**2013**) Efficient delivery of therapeutic small nucleic acids to prostate cancer cells using ketal nucleoside lipid nanoparticles J. Controlled Release 172, 954– 961 DOI: 10.1016/j.jconrel.2013.09.006
23. Immordino, M. L., Dosio, F., and Cattel, L. (**2006**) Stealth liposomes: review of the basic science, rationale, and clinical applications, existing and potential Int. J. Nanomedicine 1, 297– 315
24. Chabaud, P., Camplo, M., Payet, D., Serin, G., Moreau, L., Barthélémy, P., and Grinstaff, M. W. (**2006**) Cationic nucleoside lipids for gene delivery Bioconjugate Chem. 17, 466– 472 DOI: 10.1021/bc050162q
25. Patel, D., Kell, A., Simard, B., Xiang, B., Lin, H. Y., and Tian, G. (**2011**) The cell labeling efficacy, cytotoxicity and relaxivity of copper-activated MRI/PET imaging contrast agents Biomaterials 32, 1167– 1176 DOI: 10.1016/j.biomaterials.2010.10.013
26. Guo, S., Shen, S., Wang, J., Wang, H., Li, M., Liu, Y., Hou, F., Liao, Y., and Bin, J. (**2015**) Detection of high-risk atherosclerotic plaques with ultrasound molecular imaging of glycoprotein IIb/IIIa receptor on activated platelets Theranostics 5, 418– 430 DOI: 10.7150/thno.10020

27. Lewis, D. R., Petersen, L. K., York, A. W., Zablocki, K. R., Joseph, L. B., Kholodovych, V., Prud'homme, R. K., Uhrich, K. E., and Moghe, P. V. (**2015**) Sugar-based amphiphilic nanoparticles arrest atherosclerosis in vivo Proc. Natl. Acad. Sci. U. S. A. 112, 2693– 2698 DOI: 10.1073/pnas.1424594112
28. Sanchez-Gaytan, B. L., Fay, F., Lobatto, M. E., Tang, J., Ouimet, M., Kim, Y. T., van der Staay, S. E. M., van Rijst, S. M., Priem, B., Zhang, L., Fisher, E. A., Moore, K. J., Langer, R., Fayad, Z. A., and Mulder, W. J. M. (**2015**) HDL-Mimetic PLGA Nanoparticle To Target Atherosclerosis Plaque Macrophages Bioconjugate Chem. 26, 443– 451 DOI: 10.1021/bc500517k
29. Rader, D. J. and Daugherty, A. (**2008**) Translating molecular discoveries into new therapies for atherosclerosis Nature 451, 904– 913 DOI: 10.1038/nature06796
30. Arehart, E., Stitham, J., Asselbergs, F. W., Douville, K., MacKenzie, T., Fetalvero, K. M., Gleim, S., Kasza, Z., Rao, Y., Martel, L., Segel, S., Robb, J., Kaplan, A., Simons, M., Powell, R. J., Moore, J. H., Rimm, E. B., Martin, K. A., and Hwa, J. (**2008**) Acceleration of Cardiovascular Disease by a Dysfunctional Prostacyclin Receptor Mutation Circ. Res. 102, 986– 993 DOI: 10.1161/CIRCRESAHA.107.165936
31. Arehart, E., Gleim, S., Kasza, Z., Fetalvero, K. M., Martin, K. A., and Hwa, J. (**2007**) Prostacyclin, Atherothrombosis, and Cardiovascular Disease Curr. Med. Chem. 14, 2161– 2169 DOI: 10.2174/092986707781389637
32. Kawabe, J.-I., Ushikubi, F., and Hasebe, N. (**2010**) Prostacyclin in Vascular Diseases - Recent Insights and Future Perspectives Circ. J. 74, 836– 843 DOI: 10.1253/circj.CJ-10-0195
33. Jacobin-Valat, M. J., Laroche-Traineau, J., Lariviere, M., Mornet, S., Sanchez, S., Biran, M., Lebaron, C., Boudon, J., Lacomme, S., Cérutti, M., and Clofent-Sanchez, G. (**2015**) Nanoparticles functionalised with an anti-platelet human antibody for in vivo detection of atherosclerotic plaque by magnetic resonance imaging Nanomedicine 11, 927– 937 DOI: 10.1016/j.nano.2014.12.006
34. Roy, C. E., Kauss, T., Prevot, S., Barthélémy, P., and Gaudin, K. (**2015**) Analysis of fatty acid samples by hydrophilic interaction liquid chromatography and charged aerosol detector J. Chromatogr. A 1383, 121– 126 DOI: 10.1016/j.chroma.2015.01.046
35. Oumzil, K., Khiati, S., Grinstaff, M. W., and Barthélémy, P. (**2011**) Reduction-triggered delivery using nucleoside-lipid based carriers possessing a cleavable PEG coating J. Controlled Release 151, 123– 30 DOI: 10.1016/j.jconrel.2011.02.008
36. Khiati, S., Pierre, N., Andriamanarivo, S., Grinstaff, M. W., Arazam, N., Nallet, F., Navailles, L., and Barthélémy, P. (**2009**) Anionic Nucleotide-Lipids for In Vitro DNA Transfection Bioconjugate Chem. 20, 1765– 1772 DOI: 10.1021/bc900163s